III-5

Life, Earth and Planetary Sciences

High light

BL4U

Spring in the Arctic Ocean during ARTofMELT Expedition: A STXM/NEXAFS Analysis of Aerosol Particle Composition and Mixing State

N. Fauré[1], T. Araki.[2], E. S. Thomson[1] and X. Kong[1]

[1]*Department of Chemistry and Molecular Biology, University of Gothenburg, SE-412 96 Gothenburg, Sweden*

[2]*UVSOR Synchrotron, Institute for Molecular Science, Okazaki 444-8585, Japan*

The Arctic region is warming two to four times faster than the rest of the globe, a phenomenon called Arctic Amplification (AA). The enhanced warming pace in the Arctic arises from several sources including cloud feedback effects. In winter, aerosol particles in the Arctic mainly come from transport, while summer is dominated by local sources. These particles eventually act as Cloud Condensation Nuclei (CCN) or Ice Nucleating Particles (INP), modifying cloud formation and properties.

Spring in the Arctic is characterized by mixed sources of aerosol particles, transitioning from the transport-dominated regime (winter) to local sources (summer) due to reduced sea ice extent. The concentration, composition, vertical distribution, and CCN/INP efficiency of spring-time aerosol particles are poorly constrained due to a lack of measurements at this time of the year, especially over the Arctic Ocean. To fill this data gap, the Atmospheric Rivers and the onseT of sea ice MELT (ARTofMELT) expedition took place from May to June 2023 in the Arctic Ocean onboard the Swedish icebreaker Oden.

During this expedition, impactors were placed at the edge of sea ice, next to open leads, to collect sea spray aerosol particles for STXM/NEXAFS analysis. A microscopic image of the particles collected on June 8, 2023, displayed in Fig.1(a), reveals different particle morphologies. A more detailed investigation with STXM/NEXAFS was performed on particles I and II in Fig.1(b).

In Fig.2, similar spectra are obtained for all the regions investigated, highlighting the presence of sulfate (SO_4^{2-}) in both particles. This result does not come as a surprise as SO_4^{2-} makes up the highest concentration of particulate species measured in the Arctic.

In Fig.3, the NEXAFS spectra of the particles and regions investigated show significant discrepancies. The N-Kedge spectra revealed a higher intensity of the N=O bond at 401 eV in region 2, while particle I shows a significant amount of N-H bonding species at 405.5 eV, probably ammonium (NH_4^+). No signal is observed for C-Kedge and K-Ledge for particle I, which is likely to be mainly made of ammonium sulfate $(NH_4)_2SO_4$. Particle II displays a strong intensity of oxidized carbon at 288.2 eV and 290.5 eV for all regions, while K^+ is only observed in region 2.

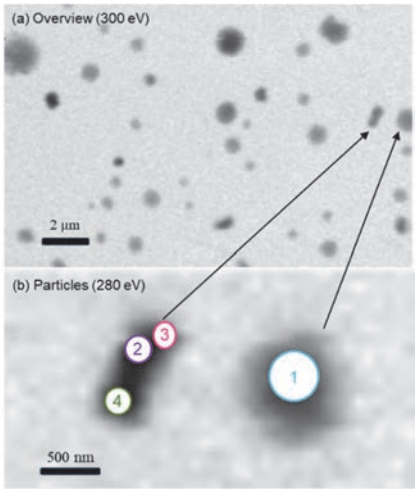

Fig.1. (a) Overview scan of particles collected next to open lead in the Arctic Ocean and (b) particles of interest for STXM/NEXAFS.

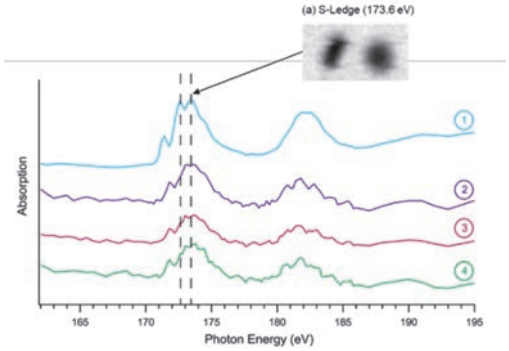

Fig.2. Sulfur L-edge NEXAFS spectra.

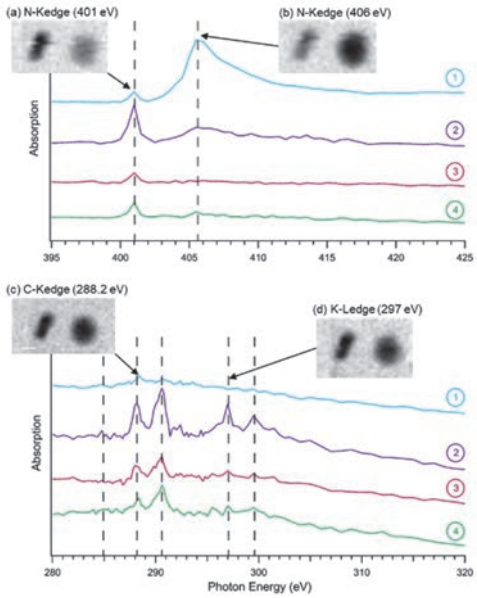

Fig.3. Nitrogen K-edge, carbon K-edge, and potassium L-edge NEXAFS spectra.

BL1U

Optical Activity Emergence of Organic Molecules Induced by Circularly Polarized Lyman-α Light Irradiation and Magnetic Field Application

M. Kobayashi[1], J. Takahashi[2], H. Ota[3], K. Matsuo[4], G. Fujimori[5], Y. Taira[3], M. Katoh[3,4], K. Kobayashi[5,6], Y. Kebukawa[6] and H. Nakamura[1]

[1]*National Institute for Fusion Science, Toki 509-5292, Japan*
[2]*Self-organization Science Research Center, Doshisha University, Kyotanabe 610-0321, Japan*
[3]*UVSOR Synchrotron Facility, Institute for Molecular Science, Okazaki 444-8585, Japan*
[4]*Hiroshima Synchrotron Radiation Center, Hiroshima University, Higashi-Hiroshima 739-0046, Japan*
[5]*Department of Chemistry and Life Science, Yokohama National University, Yokohama 240-8501, Japan*
[6]*Department of Earth and Planetary Sciences, Tokyo Institute of Technology, Meguro-ku, Tokyo 152-8550 Japan*

The biomolecules of the living organisms on the earth consist of left-handed (L-isomer) amino acids, known as the homochirality of life, and it remains as one of the most mysterious problems in the study of origin of life. One of the possible explanations of the enantiomer excess is selective photolysis caused by radiation field in space, "Cosmic scenario" [1]. For example, it has been proposed that circularly polarized light (CPL) from star-forming region is irradiated onto interstellar and circumstellar organic molecules and that causes selective photolysis resulting in the enantiomer excess of the biomolecules. In order to verify the cosmic scenario, we have conducted experiments to irradiate CPL onto amino acids. In this study, particularly we have focused on Lyman-α (121.6 nm), which has been recently observed in star-forming regions, and thus is one of the most possible candidates for the cause of the selective photolysis when it is circularly polarized [2]. In addition, we have also focused on the magneto-optical effects on the organic molecules to take into account of the magnetic field in space.

The experiments have been carried out at the undulator beamline BL1U of UVSOR-III [3], Institute for Molecular Science, where an irradiation system has been newly developed to realize the Lyman-α CPL irradiation and the application of magnetic field simultaneously. In the present experiments, the thickness of the MgF_2 window, which is for vacuum isolation between the beam line and the sample chamber, down to 0.5 mm to reduce the attenuation. The higher order light with 10 nm or less contained in the original beam was attenuated by a focusing mirror situated upstream of the MgF_2 window to avoid the damage of the window materials, which leads to further decrease of the transmittance of the window. At the beamline BL1U, left and right circularly polarized light with a peak at 121.6 nm was extracted, and was injected into the vacuum chamber, where the amino acid sample was installed, through a gate valve with the MgF_2 window. DL-alanine, racemic mixture crystal of alanine (the chiral amino acid with the simplest structure), was used as an organic molecule specimen. A thin DL-alanine film with a thickness of about 100 nm was formed on a CaF_2 substrate by vacuum evaporation. The magnetic field was applied in parallel or anti-parallel to the light axis with a strength of 0.7 T. The circular dichroism (CD) spectrum was measured before and after the irradiation at the synchrotron radiation CD beam line BL-12 of Hiroshima Synchrotron Radiation Center (HiSOR), Hiroshima University [4], and with CD spectrometer in Institute for Molecular Science.

Figure 1 shows spectra of DL-alanine films after the CPL irradiation. We clearly observe optical activity induced by the CPL irradiation, which shows opposite sign in the optical anisotropy factor g between R- and L-CPL It is also found that the g values slightly change with the magnetic field application to the CPL irradiation, irrespective of the direction of the magnetic field (not shown in the figure). The results suggest a certain impact of the magnetic field application on the optical activity caused by the CPL irradiation.

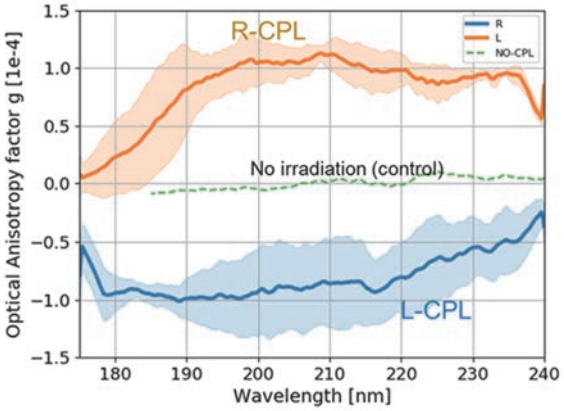

Fig. 1. Optical anisotropy factor g of the DL-Alanine film after CPL irradiation. The CD spectra is normalized with absorbance to compensate different film thickness from sample to sample.

[1] J. Takahashi and K. Kobayashi, Symmetry **11** (2019) 919.
[2] A. Sato *et al*., Astrobiology **23** (2023) 1.
[3] H. Ota *et al*., J. Phys. Conf. Ser. **2380** (2023) 012003.
[4] K. Matsuo and K. Gekko, Bull. Chem. Soc. Jpn. **86** (2013) 675.

BL1U

Toward Observation of the Interaction between Ultraviolet Optical Vortex and Biomaterials

K. Matsuo[1,2,3], R. Imaura[2], S. Hashimoto[2], Y. Nishihara[3] and M. Katoh [1,2,3,4]
[1]*Hiroshima Synchrotron Radiation Center, Hiroshima University, Higashi-Hiroshima 739-0046*
[2]*Graduate School of Advanced Science and Engineering, Hiroshima University, Higashi-Hiroshima 739-8526 Japan*
[3]*School of Science, Hiroshima University, Higashi-Hiroshima 739-8526, Japan*
[4]*UVSOR Synchrotron Facility, Okazaki 444-8585, Japan*

Recently, the interaction of chiral materials with the optical vortex, which has an orbital angular moment (OAM, $l = \pm1, \pm2, \pm3, \cdots$), is gaining attention because the combinations of vortex retarder and laser in the visible region made it possible to observe the difference between the absorption of left- and right-optical vortex (vortex dichroism) like circular dichroism. Some papers have reported the negative experimental results for the existence of vortex dichroism, but some positive results have been obtained in the absorption and reflection experiments for the oriented materials aligned on the metal substrate [1] and nanostructures [2]. Further, the optical vortex in the hard-X-ray generated by synchrotron radiation (SR) also clearly showed the vortex dichroism for the metal complex [3]. Although the generation of optical vortex with continuous light in the UV region below 300 nm, which wavelength has large interaction with the chromophores of biomaterials, was difficult due to the limitations of laser performance, recently the helical undulator which is one of the SR instruments to generate the circularly-polarized light has been recognized as a generator tool of the optical vortex in the wide range of wavelength (far-UV, vacuum-ultraviolet (VUV), and extreme-UV (EUV) regions) without any optical elements [4, 5], opening new pathway for the studies on the interaction between biomaterials and optical vortex in the UV region. However, successful observations of vortex dichroism are limited to the three reports mentioned above, and the mechanism remains fully unknown. Hence, in this study, we constructed the experimental systems for observing the interaction between biomaterials and optical vortex in the UV region using SR undulator beamline BL1U of the UVSOR-III storage ring.

Figure 1a shows the experimental setup for observing the absorption patterns of the optical vortex (OAM, $l = \pm1$) using the second-harmonic radiation from the helical undulator. The SR light passed through an iris diaphragm, and reached the lens and a multi-channel monochromator, which can detect the signals in the wide range of wavelength from visible to UV regions.

The parameters of optical vortex from helical undulator are ($s = +1, l = +1$) or ($s = -1, l = -1$). So, we put the wire grid filter before the sample to modulate the circularly polarized light to the linearly polarized light (Fig. 1a). The spectrum of vortex dichroism in the case of ($s = 0, l = +1$) and ($s = 0, l = -1$) for *d*-10 camphor sulfonic acid (ACS) was observed in the wavelength region from 305 to 270 nm using the multi-channel monochromator. As preliminary results, it seems that the spectrum of vortex dichroism and linear dichroism (with wire grid filter) of ACS are different around 270 nm but the differences are mostly within errors. However, larger differences were obtained when using the optical vortex in the case of ($s = +1, l = +1$) and ($s = -1, l = -1$) (without wire grid filter) although we need to further investigate the difference between the absorptions of left- and right optical vortex in more details.

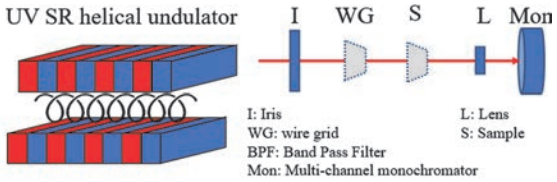

Fig. 1. Experimental setup for observing optical voltex using the second-harmonic radiation from the helical undulator.

[1] W. Brullot *et. al*., Sci. Adv. **2** (2016) e1501349.
[2] J. Ni *et. al*., ACS Nano **15** (2021) 2893.
[3] J.R. Rouxel *et. al*., Nat. Photonics **16** (2022) 570.
[4] M. Katoh *et. el*., Sci. Rep. **7** (2017) 6130, Phys. Rev. Lett. **118** (2017) 094801.
[5] T. Kaneyasu *et. al*., Phys. Rev. A: At. Mol. Opt. Phys. **95** (2017) 023413.

BL3U

X-ray Absorption Spectra of Lipid Bilayer Membranes in Aqueous Solutions and Its Dependence on Cation Concentration

R. Tero [1], Y. Kinjo[1] and M. Nagasaka[2]
[1]*Toyohashi University of Technology, Toyohashi 441-8580, Japan*
[2]*Institute for Molecular Science, Okazaki 444-8585, Japan*

The lipid bilayer, which is a self-assembled structure of amphiphilic lipid molecules, is the fundamental structure of biomembranes such as cell membranes. Transportation of materials, information, and energy into and out of cells proceeds at the cell membrane in the presence of electrolytes. Ions in the aqueous solution significantly influence to physical properties and structures of lipid bilayers. Phosphatidylcholine (PC) is the most abundant lipid of eukaryotic cell membranes. Cations bind to the phosphate and carbonyl groups of PC. However, affinity of cations to PC and effects of cations to molecular orientation are still controversy especially in the fields of theoretical simulations. We aim to clarify the coordination states of cations to lipid molecules in aqueous solutions experimentally, by means of X-ray absorption spectroscopy (XAS) [1, 2].

Supported lipid bilayers (SLBs) of dioleoyl-PC (DOPC) were formed on the Si_3N_4 membranes of the XAS flow cell [1] by the vesicle fusion method in a buffer solution (NaCl 100 mM, HEPES 25 mM/ pH 7.4 NaOH). The Na^+ concentration ([Na^+]) was varied by exchanging the buffer solution in the flow cell in in the range of [Na^+] = 2.1 – 510.4 mM. The O-K edge XAS spectra of SLB were obtained at the energy range of 527 – 535 eV. The X-ray incident angle of 35º. The XAS spectrum of the Si_3N_4 membrane without SLB was subtracted from that with SLB.

The O K-edge spectrum of DOPC appeared at 531 - 533 eV [2, 3]. It is consisted of 1s→π* transitions of double-bond oxygens in the phosphate and carbonyl groups on the PC headgroup: two components attributed to the P=O in the former, and one component attributed to the latter. We measured XAS spectra at the X-ray incident angle (T) of 35º. We obtained a specific dependence of the P=O peak at the lower energy on [Na^+]: its position was little affected by [Na^+] in the range of 2.1 – 10.4 mM and shifted to higher energy by 0.4 eV at [Na^+] = 50.4 mM. The position showed slight change at [Na^+] > 110.4 mM. The results show the Na^+ coordination to the phosphate group of DOPC and its dependence of [Na^+].

The inner-shell quantum chemical calculation [4] of O K-edge spectrum of P=O was performed based on the atomic positions obtained from the theoretical calculation of the DOPC bilayers in aqueous conditions at [NaCl] = 2 – 100 mM (Fig. 1). The inner-shell spectra of oxygen atoms in the phosphate group showed high-energy shift depending on the distance from Na^+ that was consistent with the experimental results. We also found that the peak intensity also depended on the distance between Na^+ and the oxygen atom in the P=O group. These results indicate that the ion coordination on lipid molecules is evaluated by the XAS spectra in water.

We have confirmed that the XAS spectra of DOPC were reproducibly obtained with a sufficient S/N ratio at the beam current condition of 200 mA in this year. The effects of the cation species on the XAS spectra of DOPC bilayer are also investigated.

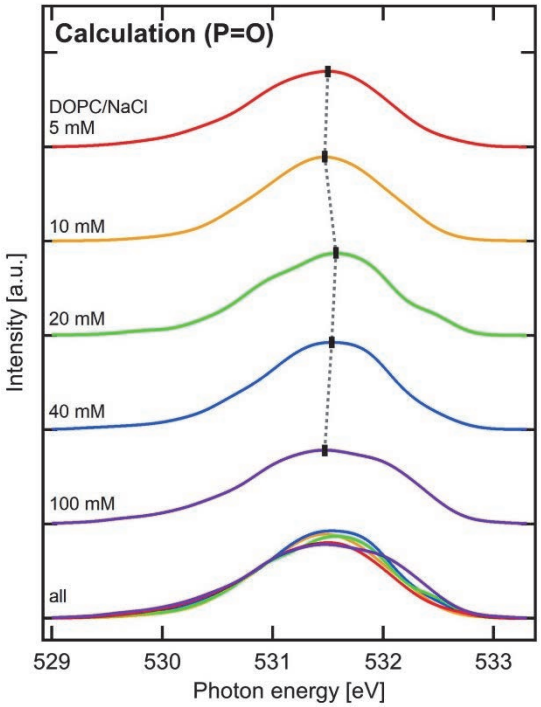

Fig. 1. The inner-shell spectra of oxygen atoms in the phosphate groups in the DOPC-bilayers at various NaCl concentrations. The peak positions are indicated with dotted lines. The overlapped spectra are shown at the bottom for comparison in peak intensity.

[1] M. Nagasaka *et al.*, J. Electron. Spectrosc. Relat. Phenom. **224** (2018) 93.
[2] R. Tero, Y. Kinjo and M. Nagasaka, UVSOR Activity Report **49** (2022) 151.
[3] R. Tero, Y. Kinjo and M. Nagasaka, UVSOR Activity Report **50** (2023) 165.
[4] M. Nagasaka, J. Chem. Phys. **158** (2023) 024501.

BL3U

Laser Excited Photochemical Reaction of Dissolved Oxygen on Lipid Bilayer Measured by Oxygen K-Edge XAS

F. Kumaki[1], M. Nagasaka[2, 3], Y. Kinjo[4], R. Tero[4], Y. Okano[2] and J. Adachi[1, 5]

[1]*Institute of Materials Structure Science, High Energy Accelerator Research Organization, Tsukuba 305-0801, Japan*

[2]*Institute for Molecular Science, Okazaki 444-8585, Japan*

[3]*Molecular Science Program, Graduate Institute for Advanced Studies, SOKENDAI, Okazaki 444-8585, Japan*

[4]*Toyohashi University of Technology, Toyohashi 441-8580, Japan*

[5]*Materials Structure Science Program, Graduate Institute for Advanced Studies, SOKENDAI, Tsukuba 305-0801, Japan*

When photosensitizers such as porphyrin dyes are photoexcited, singlet oxygen ($^1O_2$) with high reactivity is generated owing to the energy transfer to the triplet oxygen ($^3O_2$). Photodynamic therapy, in which photosensitizers are injected into living bodies to destroy cancer cells by generating $^1O_2$, has recently gained attention [1]. We have attempted to elucidate the elementary process of $^1O_2$ generation via photoreaction in biological membranes in detail using O K-edge X-ray absorption spectroscopy (XAS) since 2021 [2, 3].

To measure the electronic state of $^1O_2$ generated in lipid layers including photosensitizers, time-resolved liquid XAS system by the combination of soft X-ray pulses (530 eV, 128 ps) and visible laser pulses (400 nm) was used at BL3U. The synchrotron radiation pulse duration of about 100 ps at the UVSOR facility would be short enough to probe the reaction dynamics of $^1O_2$ which has a lifetime of about 3 μs dissolved in liquid [4].

The liquid XAS system at BL3U was used to measure the O K-edge XAS spectra of dissolved oxygen in lipid layers. The liquid layer in the cell was sandwiched between two Si_3N_4 membranes with lipid bilayers. We established the method to measure O K-edge XAS spectra of dissolved oxygen kept on lipid bilayers [2]. For improving the signal-to-noise ratio of the spectra from the previous measurement, several lipid bilayers were added beforehand to increase the amount of dissolved oxygen in the liquid cell. The chlorophyll-*a*, which is a photosynthetic pigment to the lipid bilayers as a photosensitizer, were added in the lipid bilayers. Chlorophyll-*a* was found to be an excellent dye as a model system for photoreaction in lipid bilayers.

We plan to irradiate the SHG of Ti:sapphire laser (419 nm, 0.5 mW) to the liquid cell for conducting the photoexcitation of the chlorophyll-*a*. The laser wavelength will be adjusted to match the maxima of the soret band of the chlorophyll-*a*. To observe the difference of the O K-edge XAS spectra of the dissolved oxygen due to the $^1O_2$ generated via the photoreaction of chlorophyll-*a*, we will measure the XAS spectra with and without laser irradiation simultaneously by using a gate signal synchronized with the shutter of the laser. By changing the phase of the laser, the delay from the synchrotron radiation will be shifted to find the delay at which the spectra show a large change from the spectra of the ground state.

Figure 1 shows the O K-edge XAS spectra of the lipid bilayers with adsorbed oxygen. Compared to the XAS spectrum obtained in the previous measurement (blue line), the present XAS spectrum shows the larger peak between 530 eV and 533 eV owing to the increase in the adsorption of the dissolved oxygen in the lipid bilayer. In the future, we will continue the laser excited photochemical reactions of dissolved oxygen using the present lipid bilayers.

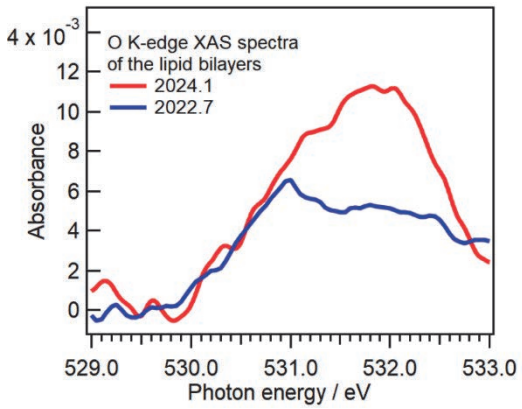

Fig. 1. The O K-edge XAS spectra of the lipid bilayers with adsorbed oxygen. The spectrum obtained in the previous measurement are also shown for the comparison of the present measurement.

[1] M. Ethirajan *et al.*, Chem. Soc. Rev. **40** (2011) 340.
[2] F. Kumaki *et al.*, UVSOR Activity Report **49** (2022) 118.
[3] F. Kumaki *et al.*, UVSOR Activity Report **50** (2023) 123.
[4] C. A. Long and D. R. Kearns, J. Am. Chem. Soc. **97** (1975) 2018.

BL3U

Soft X-ray Absorption Spectroscopic Study of Myoglobin Heme in Solution

Y. Sugimoto[1] and M. Nagasaka[2,3]

[1]*UVSOR Synchrotron Facility, Institute for Molecular Science, Okazaki 444-8585, Japan*

[2]*Institute for Molecular Science, Okazaki 444-8585, Japan*

[3]*The Graduate University for Advanced Studies (SOKEIDAI), Okazaki 444-8585, Japan*

Heme is a complex of porphyrin and iron atom. Heme binds to proteins and serves as an active center for a wide variety of activities, including oxygen transport or electron transfer. One of the best-known heme proteins is myoglobin in muscle, that binds and stores oxygen to the iron atoms of heme. Myoglobin was the first protein whose structure was determined by X-ray crystallography [1] and have been studied in various ways. On the other hand, spectroscopic study using soft X-rays have not been widely applied to observe heme and proteins. This is because soft X-rays are strongly absorbed by air and water, making it difficult to apply spectroscopic measurements of proteins in solution.

Soft X-ray absorption spectroscopy (XAS) of liquid samples has been developed using a liquid cell at soft X-ray beamline BL3U of UVSOR [2]. In this study, we aimed to measure the electronic structures of heme in myoglobin by using nitrogen K-edge XAS in transmission mode. Our measurement system can observe liquid samples at room temperature and atmospheric pressure. In heme, the iron atom is coordinated to the nitrogen atom of the porphyrin. It is important to clarify the electronic structure of the nitrogen atoms surrounding the metal center as well as the iron atoms responsible for oxygen binding.

The experiments were carried out in BL3U. Myoglobin solution was prepared to be 1 mM in phosphate buffer. We prepared oxygenated myoglobin (oxyMb), deoxygenated myoglobin (deoxyMb), and metmyoglobin (metMb, oxidized to Fe^{3+}). These samples were checked from the UV-Visible spectroscopic measurements. SiC membranes were used as the vacuum window and the windows of the liquid cell for the measurements of the nitrogen K-edge XAS. XAS spectra were obtained by measuring the transmission intensities of soft X-rays from 395 eV to 415 eV.

Figure 1 shows the UV-Visible spectra of myoglobin in solution, which are oxyMb, deoxyMb, and metMb. From the comparison of the previous studies, we confirmed that the samples were prepared correctly for each condition. Figure 2 shows the N K-edge XAS spectra of myoglobin and bovine serum albumin (BSA) samples in solution. BSA is a protein without heme. While the signals commonly observed for both myoglobin and BSA are at ~401 eV and ~406 eV, a peak was observed at ~400 eV only in the myoglobin samples and not in BSA. This result implies that the peak at 400 eV is derived from nitrogen atoms in heme. It was also suggested that there may be an energy shift between the oxyMb and deoxyMb peaks at 400 eV.

In this experiment, the possibility of observing light elements in biological macromolecules was demonstrated under physiological conditions. Further precise measurements and spectral analysis of nitrogen K-edge XAS of heme in protein will be made.

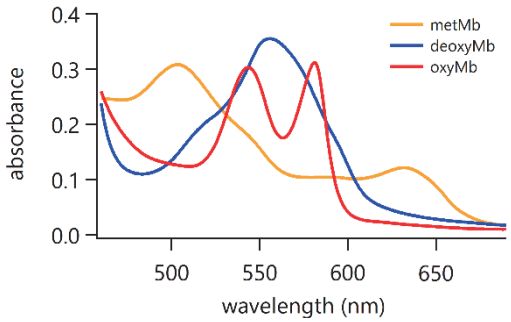

Fig. 1. UV-visible spectra of myoglobin, which are oxyMb, deoxyMb, and metMb.

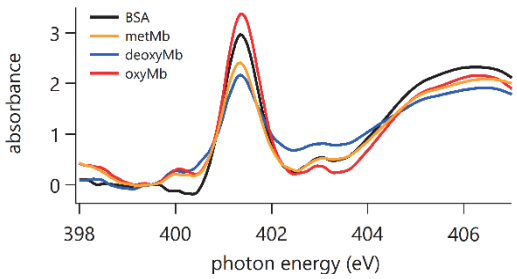

Fig. 2. N K-edge XAS spectra of myoglobin and BSA samples in solution. Each Spectrum was normalized at 399 eV.

[1] J. C. Kendrew *et al.*, Nature **181** (1958) 662.
[2] M. Nagasaka and N. Kosugi, Chem. Lett. **50** (2021) 956.

BL4U

The Effect of Freeze-Defrosting Cycles on the Spherule Size, Morphology, and Chemical Compositions of HCN Polymer

H. Yabuta[1], N. Nishii[1] and T. Araki[2]
[1]*Department of Earth and Planetary Systems Science, Hiroshima University, Hiroshima 739-8526, Japan*
[2] *UVSOR Synchrotron Facility, Institute for Molecular Science, Okazaki 444-8585, Japan*

It has been thought that organic nanoglobules in primitive small body materials, such as carbonaceous meteorites, cosmic dusts, and the returned asteroid samples, are derived from extremely cold environments in space, based on the observed enrichments of deuterium and/or nitrogen-15 (e.g., Nakamura-Messenger et al. 2006). Variations in sizes, morphologies, and chemical compositions of the organic nanoglobules could have been resulted on the meteorite parent bodies (De Gregorio et al. 2013), while they may have been altered in interstellar molecular cloud or outer solar nebula, as freeze concentration of molecules drive some organic synthesis such as HCN oligomerization under low temperature conditions (Miyakawa et al. 2002). In this study, we conducted a freeze-defrosting cycle experiment of a synthesized HCN polymer as organic nanoglobule analogue to investigate the effect of freeze-defrosting on their morphologies, size distributions, and functional group chemistry.

HCN polymer was synthesized by heating formamide (0.3 ml) at 185℃ for 72 hours (Cataldo et al., 2009). Freeze-defrosting cycle experiments of the mixture of HCN polymer (0.05 ml) and water (0.05 ml) in a screw vial were conducted. One freeze-defrosting cycle consisted of freezing at -196℃ for 10s with liquid N_2, increasing the temperature from -196℃ to −20℃ for 24 hours in refrigerator, and increasing the temperature from −20℃ to room temperature for 5 min. The experiments were conducted during 10, 20, 30, and 40 freeze-defrosting cycles. The products obtained under each condition were observed by FE-SEM (Hiroshima University) and analyzed by STXM-XANES, beam line 4U, UVSOR.

The FE-SEM observation showed that the sizes of organic microspherules in HCN polymer obtained after 10 freeze-defrosting cycles were larger than the starting HCN polymer before the experiment, while the sizes of organic microspherules after 20 freeze-defrosting cycles were smaller than the starting HCN polymer (0 cycle). A variety of morphologies, such as dumbbell-like structures, were observed from the products after 10 and 20 freeze-defrosting cycles. It should be noted that these diverse morphologies and sizes were observed in the presence of unreacted formamide, but without formamide. It is probably because formamide is ionic liquid that can dissolve the water-insoluble HCN polymer, which may have accelerated growth and division of the organic microspherules.

The STXM-XANES measurements showed that the peaks of nitrile or nitrogen heterocycles (286.7 eV), amide or carboxyls (288.2 eV) were the highest in the C-XANES spectra of the starting HCN polymer and all the products except for the product after 10 cycles. The peaks of aromatic C=C (285.2eV),alcohol or ether (289.5 eV) were the next highest. The peaks corresponding to imine (398.8 eV) and pyrrole (400.5 eV) were identified in the N-XANES spectra of all the samples, while amide peak was absent. Thus, the peak around at 288.2eV in C-XANES could be derived from carboxyls. In the products after the freeze-defrosting cycles experiment, the peak intensity of carboxyls was slightly higher than that of aromatic nitrogen. The increase of carboxyls is probably due to hydrolysis of the organic microspherules during defrosting.

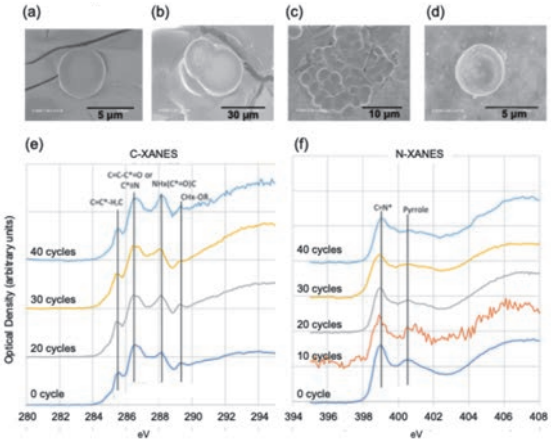

Fig. 1. SEM images of organic microspherules of HCN polymer after (a) 0, (b) 10, (c) 20, and (d) 40 cycles of freeze-defrosting experiment and (e) C- and (f) N-XANES spectra of HCN polymer before and after the freeze-defrosting cycle experiment.

[1] K. Nakamura-Messenger *et al*., Science **314** (2006) 1439.
[2] B. T. De Gregorio *et al.*, Meteorit. Planet. Sci. **48** (2013) 904.
[3] S. Miyakawa *et al.*, Origins Life Evol. Biosphere **32** (2002) 209.
[4] F. Cataldo *et al.*, J. Macromol. Sci. **46** (2021) 1039.

Aerosol Particle Mixing States in Delhi: A STXM/NEXAFS Investigation into Nighttime Growth Mechanisms

M. Wickramanayake[1], E. Tsiligiannis[1], T. Araki.[2], E. S. Thomson[1] and X. Kong[1]
[1]*Department of Chemistry and Molecular Biology, University of Gothenburg, SE-412 96 Gothenburg, Sweden*
[2]*UVSOR Synchrotron, Institute for Molecular Science, Okazaki 444-8585, Japan*

Delhi, one of the most polluted global capitals, faces a dire air pollution crisis, particularly during winter when fine particulate matter (PM2.5) levels often exceed 500 $\mu g \cdot m^{-3}$, which is over 30 times than the WHO's recommended limit of the 24-hour average value (15 $\mu g \cdot m^{-3}$). This pollution, significantly contributed to by vehicular emissions, industrial activities, and biomass burning, creates a dense winter haze under the nocturnal conditions of the Indo-Gangetic plain. The diurnal nighttime temperature decreases, and humidity increase leads to the accumulation and growth of particulates, adversely affecting visibility and public health. Despite research efforts, the chemical processes driving nocturnal particle growth remain unclear, posing a challenge to environmental health in the region.

To address this, measurements were conducted in Delhi during February and March 2023, collecting PM samples on TEM grids for STXM/NEXAFS analysis to study particle mixing states. Figure 1 displays a STXM image of aerosol particles collected on a heavy haze day, February 27, 2023, at 14:26. The particles exhibit a diverse range of morphologies, suggesting they are externally mixed, with distinct differences observable among them. Notably, in the upper left corner of the image, there is an agglomeration of soot particles.

In Fig. 2, a focused examination of a specific central area from Fig. 1 is presented for four different photon energy levels. These levels correspond to the pre-edge of the carbon K-edge at 280 eV, the C=C bond at 285.2 eV, the C=O bond at 288.2 eV, and the potassium L-edge at 297.2 eV, respectively. These detailed views reveal the presence of several particles that absorb differently at these energy levels. At 285.2 eV, particles (1) and (2) are visible, indicating the presence of soot, which is typically generated from combustion processes. At 288.2 eV, a larger particle (3) becomes more absorbing, predominantly consisting of organic materials featuring the carbonyl group (C=O). Finally, at 297.2 eV, potassium elements are highlighted at their L-edge, with the central portion (4) of one particle showing a pronounced response.

Figure 3 presents the NEXAFS spectra for the carbon K-edge and potassium L-edge of the four distinct particles, illustrating the internal mixing state of aerosols in Delhi. The comprehensive spectra analysis reveals a significant presence of potassium across numerous particles not detailed in this report, indicating biomass burning as a key source of air pollution in the city. Potassium serves as a widely recognized marker for biomass combustion. The possible diverse hygroscopic and chemical properties of these particle types suggest they absorb water and other vapors, particularly at night. This absorption contributes to their nocturnal growth, a unique phenomenon observed in Delhi's atmospheric conditions.

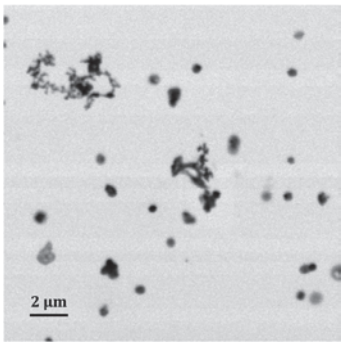

Fig. 1. An overview scan of Delhi particles acquired at a photon energy of 300 eV.

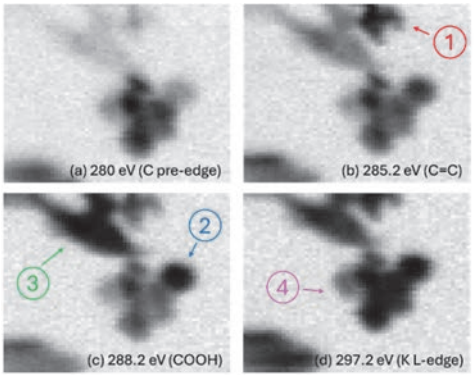

Fig. 2. Images taken at four photon energies.

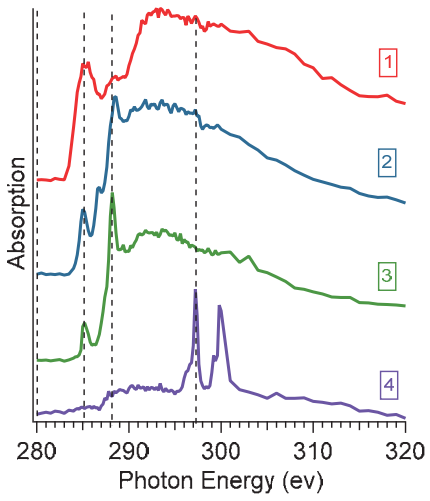

Fig. 3. Carbon K-edge and potassium L-edge NEXAFS spectra.

BL4U

STXM Characterization of Salla Disease Patient Fibroblasts

T. Mansikkala[1,2], I. Miinalainen[2], S. M. Kangas[3], R. Hinttala[3,4], J. Uusimaa[3,5], M. Huttula[1] and M. Patanen[1,2]

[1]*Nano and Molecular Systems Research Unit, PO Box 3000, 90014 University of Oulu, Finland*
[2]*Biocenter Oulu, PO Box 5000, 90014 University of Oulu, Finland*
[3]*Research Unit of Clinical Medicine and Medical Research Center, Oulu University Hospital and University of Oulu, 90014 Oulu, Finland*
[4]*Transgenic and Tissue Phenotyping Core Facility, PO Box 5000, 90014 University of Oulu, Finland*
[5]*Children and Adolescents, Oulu University Hospital, 90029 Oulu, Finland*

In this work, we used scanning transmission X-ray microscopy (STXM) technique at BL4U beamline to study cell cultured fibroblasts of Salla disease (SD) patients and control cell lines. This work continues our previous work carried out for SD mouse model tissues [1]. Salla disease (OMIM # 604369) is caused by a variant in the *SLC17A5* gene that encodes sialin, a lysosomal membrane protein that transports sialic acid (SA) out of lysosomes. Impaired function of sialin causes the SA to accumulate. Patients with SD store approximately 10-100 times the normal amounts of free SA in their tissues [2, 3]. The goal was to see if we can show the SA accumulation in SD patient fibroblast compared to healthy control fibroblasts. We also measured both patient and control fibroblasts cultured with N-Acetyl-D-mannosamine monohydrate (ManNAc). ManNAc was used to induce SA production in both SD patient (SASD) and control human dermal fibroblasts (NHDF).

Samples were measured in two different forms. Thin sections of 150 nm thickness were prepared from cells fixed in 4 % paraformaldehyde and 2.5 % glutaraldehyde in 0.1 M phosphate-buffered saline and then embedded in TTE:MMHA. The sections were placed on copper grids with butvar membrane. Same cells were also directly grown on nickel grids with formvar membrane. These cells were fixed the same way and dried with ethanol series. This was done to have measurements of cells without any embedding material.

We could not detect differences inside the lysosomes of the cells while measuring the resin embedded thin sections. Most of the lysosomes seemed to be void of material, showing only pure resin spectra. Despite some exceptions, no trend between sample types was detected. However, we did notice a difference when comparing the averaged signals of the entire cells of different sample types. The NHDF cells cultured with ManNAc had higher absorption (optical density (OD)) around 285-285.5 eV and 288-288.5 eV. The averages for each sample type were calculated after reducing the resin spectra individually from each cell using the resin measured from the scan. The averages are shown in Fig. 1. For each cell type 4 to 6 cells were measured and used in the average. This shows that STXM can be used to measure differences in cells caused by differences in genetics and cell culture.

Fibroblasts grown directly on top of the grid were too thick to get reliable results through the thickest parts of the cells. In Fig. 2. we can see the cells grown on grid showing very little transmission in the middle of the cells. However, we were able to measure the edge areas of the fibroblasts where there was enough transmission. Differences in spectrum from these areas seemed to be mostly from the thickness differences in the sample excluding few exceptions.

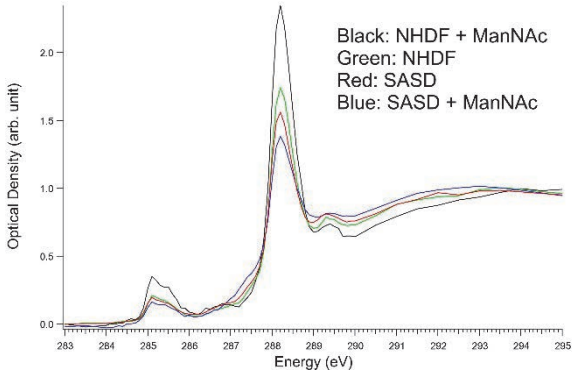

Fig. 1. Average OD of resin embedded cells after reducing the effect of resin from the sample.

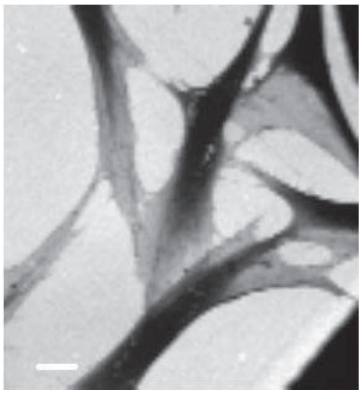

Fig. 2. Single energy (292.5 eV) transmission image of fibroblasts grown on grid. Scale bar is 10 µm.

[1] T. Mansikkala *et al.*, J. Electron. Spectrosc. Relat. Phenom. **266** (2023) 147368.
[2] P. Aula *et al.*, Arch. Neurol. **36** (1979) 88.
[3] N. Aula *et al.*, Am. J. Hum. Genet. **67** (2000) 832.

BL4U

Evaluation of Radiation-Induced NEXAFS Profile-Changes for Biomolecules in Imaging Biological Specimens

A. Ito[1], K. Shinohara[2], A. Matsuura[2], S. Toné[3], K. Tohya[4], Y. Asada[2], H. Yuzawa[5], T. Araki[5] and T. Ohigashi[6]

[1]*School of Engineering, Tokai University, Hiratsuka 259-1292, Japan*
[2]*Graduate School of Health Sciences, Fujita Health University, Toyoake 470-1192, Japan*
[3]*School of Science and Engineering, Tokyo Denki University, Hatoyama 350-0394, Japan*
[4]*Kansai University of Health Sciences, Kumatoricho 590-0482, Japan*
[5]*UVSOR Synchrotron Facility, Institute for Molecular Science, Okazaki 444-8585, Japan*
[6]*Photon Factory, Institute of Materials Structure Science, Tsukuba 305-0801, Japan*

Spectromicroscopy for molecular mapping is one of the unique applications of STXM. Since molecular distributions are calculated using a set of NEXAFS data for constituent molecules, the accuracy of the results largely depends on them. In particular, biological specimens such as our imaging targets [1-3] are supposed to be easily affected by X-ray irradiation. It is essential to estimate the modification of NEXAFS profiles as a function of X-ray absorbed dose for the quantitative molecular analysis.

In our previous report, we obtained absorbed dose dependence of mass absorption coefficient of biomolecules at specific photon energies [4]. In the present study, we extended such dose dependence profiles to every photon energy used for NEXAFS measurements. Based on this set of dose dependences, we can obtain NEXAFS at a given absorbed dose for imaging biological specimens. In addition, we can also estimate NEXAFS profiles of intact biomolecules by extrapolating the dose response curve to zero dose.

We prepared dry thin films of DNA, RNA, histone, BSA, actin monomer and nucleosome on SiN membrane. NEXAFS measurements were done for a defined area at the C, N, and O K-edges in this order, which is critical to calculate absorbed dose. The dwell time for the measurements was 6, 12 and 20 msec. For each dwell time, the scanned area was shifted to the different area to avoid additional radiation effects.

DNA spectra of mass absorption coefficient at the C, N and O K-edges were shown in Fig. 1. The blue lines were NEXAFS at the absorbed dose corresponding to each exposure for the observation of an apoptotic nucleus, while the red lines indicate NEXAFS estimated for intact DNA before exposure. Note that the absorbed dose was increased sequentially in the order from the lowest energy of the C K-edge to the highest energy of the O K-edge; for example, the dose at the starting point of the N K-edge was accumulated to the total dose of the preceding measurement at the C K-edge. The modification of the spectra does not seem to be so significant in the present imaging condition. Similar tendencies in the profile-changes to nucleic acids were found for proteins such as histone and actin.

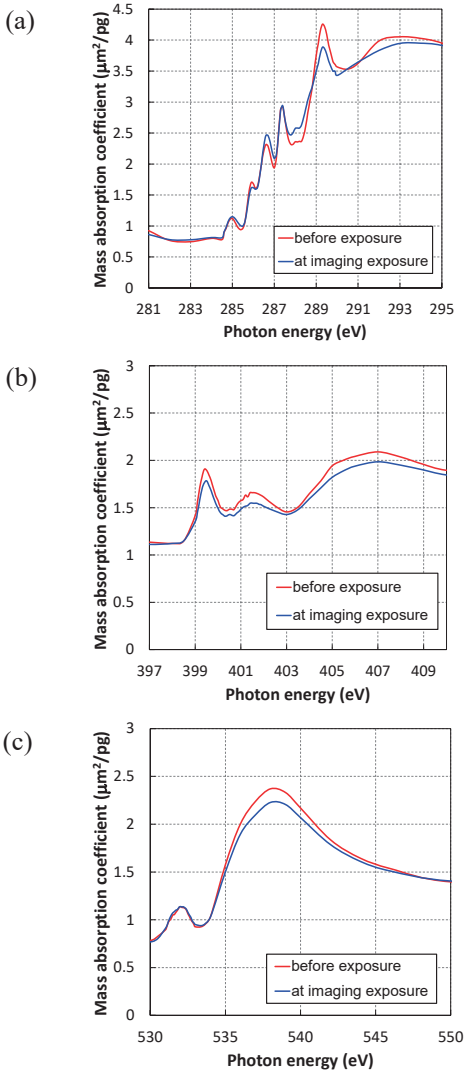

Fig. 1. NEXAFS of DNA at (a) C K, (b) N K, (c) O K-edges. Blue line: with X-ray exposure for imaging apoptotic nuclei; Red line: with no X-ray exposure.

[1] K. Shinohara *et al.*, Ultramicroscopy **194** (2018) 1.
[2] K. Shinohara *et al.*, J. X-Ray Sci. Technol. **26** (2018) 877.
[3] K. Shinohara *et al.*, Cells **8** (2019) 8.
[4] A. Ito *et al.*, UVSOR Activity Report **50** (2023) 173.

BL4U

Chemical Structures of Macromolecular Organic Matter in Ryugu Grain.

T. Matsumoto[1], T. Noguchi[2], T. Araki[3], T. Ohigashi[4], Y. Igami[2] and A. Miyake[2]
[1]*The Hakubi center for Advanced Research, Kyoto University, Kitashirakawa-Oiwakecho, Sakyo, Kyoto 606-8502, Japan*
[2]*Division of Earth and Planetary Sciences, Kyoto University, Kitashirakawa-Oiwakecho, Sakyo, Kyoto 606-8502, Japan*
[3]*Institute for Molecular Science, 38 NishigoNaka, Myodaiji, Okazaki 444-8585, Japan*
[4]*High Energy Accelerator Research Organization. 1-1 Oho, Tsukuba, Ibaraki 305-0801 Japan*

Regolith samples recovered from the C-type asteroid Ryugu show chemical and petrological characteristics similar to those of CI carbonaceous chondrites [1-3]. Insoluble organic macromolecules (IOM) in Ryugu grains are the dominant components of organic matter in Ryugu's materials [3]. The chemical structures, distributions, and morphologies of the macromolecular organic matter can be tracers of the evolution of organic materials in the interstellar medium, the protosolar disk, and the aqueous environment in the parent body of Ryugu [3]. In this study, we focused on carbon-rich regions in a Ryugu grain and examined the spatial relationship between organic materials and phyllosilicates, together with their chemical features.

A Ryugu grain from the chamber A (grain No. A0142) was distributed by JAXA. Electron-transparent sections were extracted from the regions of interest using a focused ion beam system (FIB Helios NanoLab G3 CX). Scanning transmission X-ray microscopy (STXM) imaging was performed to obtain X-ray absorption near edge structure (XANES) spectra from the sections. The bonding structure of carbon was investigated using XANES spectra at the carbon K-edge (at 280 eV-320 eV). After STXM analysis, the sections were observed using field-emission transmission electron microscope (TEM) (JEOL JEM2100F).

We investigated the largest carbon-rich region with approximately 17×8×9 μm in size (Fig.1ab). Carbon-XANES spectra of the carbon-rich region include major peaks of aromatic carbon (285 eV) and carboxyl carbon (288.5 eV), and those of phyllosilicate matrix in the vicinity of the carbon-rich region show peaks of aromatic carbon (285 eV), carboxyl carbon (288.5 eV), aliphatic carbon (287.5 eV), and carbonates (290.4 eV). TEM analysis showed that organic materials and fibrous phyllosilicates are finely intermixed in the carbon-rich region. Hereafter, we call the carbon-rich region as the carbon-phyllosilicate aggregate (CPA). Distinct morphologies of organic materials, such as the organic globules, were not identified in the CPA. The surrounding matrix consists mainly of fibrous phyllosilicates, magnetite, iron sulfides, and carbonates. High-resolution TEM images showing layered structures of the fibrous phyllosilicates (Fig. 1c) enabled us to investigate the interlayer distance of the phyllosilicates. The majority of the fibrous phyllosilicates in the CPA and the matrix have interlayer distances of 0.7~0.75nm, and 1.0-1.2nm. These values correspond to typical interlayer distances of serpentine and saponite in Ryugu samples, respectively [2]. On the other hand, fibrous phyllosilicates with interlayer distances of 1.23-1.35 nm were occasionally observed in the CPA and in the matrix close to the carbon-rich region (Fig.1c).

The enrichment of aromatic and carboxylic carbon in the XANES spectra from the CPA is similar to the spectral features of highly-aromatic or aromatic macromolecular carbon in Ryugu samples [3]. The concentration of aromatic organic matter may have occurred by redistribution and/or synthesis of organic matter during fluid activity in the parent body. It is also possible that large chunks of organic matter have been incorporated during the initial accretion of the parent body, in the form of primitive materials originated from the outer solar system [7]. The appearance of aliphatic carbon in the matrix is consistent with the previous XANES study of Ryugu samples, in which aliphatic organics were detected in association with phyllosilicates [8]. Previous X-ray diffraction measurements of Ryugu samples detected 001 reflection of smectite at 1.26 nm [4]. The relatively large interlayer distance was interpreted as the expansion of the interlayer space due to the presence of organic molecules [4]. The spatial relationship between the CPA and the possibly organic-bearing phyllosilicates suggests that macromolecular organic matter could have interacted with surrounding phyllosilicates during aqueous alteration, as suggested by analyses of carbonaceous chondrites [9, 10].

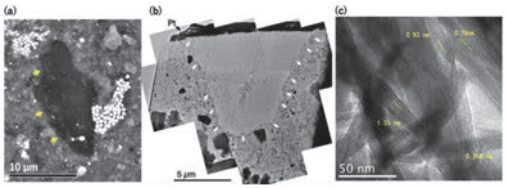

Fig. 1. The carbon-rich region of Ryugu grain (A0142). SEM image (a) and bright-field TEM image (b) of the carbon-phyllosilicate aggregate (CPA). (c) High-resolution TEM image of fibrous phyllosilicates near the CPA.

[1] T. Yokoyama *et al*., Science **379** (2022) eabn7850.
[2] T. Nakamura *et al*., Science **379** (2022) eabn8671.
[3] H. Yabuta *et al*., Science **379** (2023) eabn9057.
[4] J.-C. Viennet *et al*., Geochem. Perspect. Lett. **25** (2023) 8.
[5] Damien *et al*., Meteorit. Planet. Sci. under review.
[6] C. Pilorget *et al*., Nat. Astron **6** (2022) 221.
[7] J. Duprat *et al*., Science **328** (2010) 742.
[8] M. Ito *et al*., Nat. Astron **6** (2020) 1163.
[9] L.A.J. Garvie and P.R. Buseck, Meteorit. Planet. Sci. **42** (2007) 2111.
[10] C.L. Guillou *et al*., Geochim. Cosmochim. Acta **131** (2014) 368.

BL4B

Development of Contact X-ray Microscope for Biological Sample

H. Iwayama[1,2] and R. Sasaba[1,3]

[1]*UVSOR Synchrotron Facility, Institute for Molecular Science, Okazaki 444-8585, Japan*

[2]*School of Physical Sciences, The Graduate University for Advanced Studies (SOKENDAI), Okazaki 444-8585, Japan*

[3]*Graduate School of Frontier Biosciences, Osaka University, Suita 565-0871, Japan*

Observing the structure of biological samples using an optical microscope is life science's most basic research method. In synchrotron radiation, a wide range of light can be used, including visible light and THz light, infrared light (IR), vacuum ultraviolet light (VUV), and X-rays. Light-matter interactions depend on its wavelength. For IR, VUV, and SX regions, molecular vibration excitation, valence-electron ionization, and core-electron ionization occur. Thus, microscopy with different wavelengths enables us to see other structures. In particular, in the X-ray region, resonant energies for core electrons depend on their element and chemical states, making structures for each element and chemical state possible. Soft X-ray regions (100 ~ 2000 eV) include resonant energies for carbon, nitrogen, oxygen, phosphorus, sulfur, etc., essential to life science.

There are various imaging methods that use X-rays, such as scanning transmission X-ray microscopy and X-ray ptychography. Recently, we began developing a contact X-ray microscope. In this method, a sample such as a cell is irradiated with X-rays, and the transmitted light is observed using a scintillator to image a projected image. The principle is the same as that of conventional X-ray photography. Although the spatial resolution of this method is roughly one μm and inferior to scanning transmission soft X-ray microscopy and X-ray ptychography, it is effortless and free of chromatic aberration because it does not require sophisticated focusing optics.

In this work, we developed a contact X-ray microscope at UVSOR BL4B. Figure 1 shows a schematic drawing of our contact X-ray microscope. A sample of oral epithelial cells was placed on a Ce: YAG scintillator and sealed with a Si_3N_4 membrane (100 nm thick). The transmitted soft X-rays are converted into visible light emission by the scintillator. The scintillator light emission image is observed by an optical lens (Asahikogaku, AZ10-100E) on the atmospheric side and detected by a CMOS camera (Hamamatsu Photonics, ORCA Flash 4.0 V3). The optical lens's NA, magnification, and working distance are 0.2, x15, and 100 mm, respectively.

We took 400 images for photon energies ranging from 280 to 320 eV (0.1 eV step). Typical images of an oral cell are shown in Fig. 2. An exposure time is 10 seconds. By examining the image's energy dependence, we obtained an X-ray absorption fine structure (XAFS) spectrum for each pixel. Since the image in Figure 2 is 300 pixels x 300 pixels, it corresponds to 90,000 XAFS spectra. Then, we classify the cell structure from the spectral structure for each pixel. However, it isn't easy to manually classify a large amount of spectra, so we are developing an analysis method that uses machine learning, such as KMEAN++, to classify the spectrum of each pixel. In the future, we will create a new structural analysis of non-stained biological samples with a contact X-ray microscope and its analysis method.

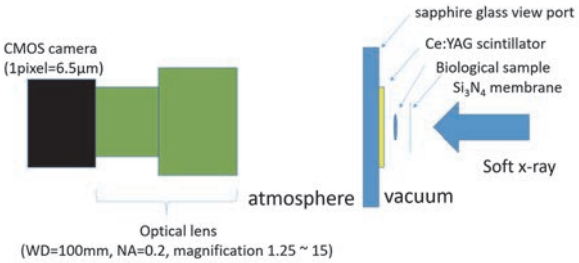

Fig. 1. Schematic drawing of contact X-ray microscope at BL4B.

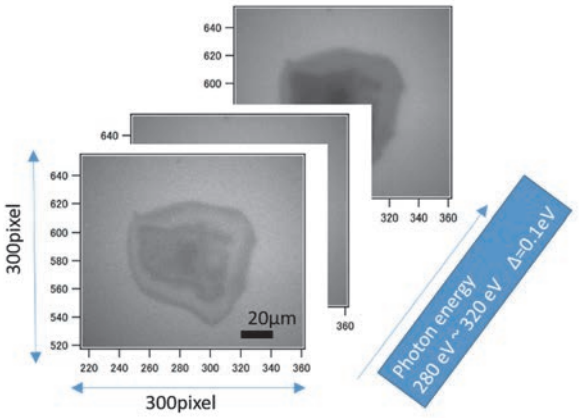

Fig. 2. Typical images of an oral epithelial cell by the contact X-ray microscope.

III-5

BL6B

Development of the Super Continuum Laser-Based Infrared Spectro-Microtomography for the Three-Dimensional Imaging of Extraterrestrial Organic Matter

H. Yabuta[1], Y. Ikemoto[2], F. Teshima[3], and K. Tanaka[3]

[1]*Department of Earth and Planetary Systems Science, Hiroshima University, Hiroshima 739-8526, Japan*
[2]*Japan Synchrotron Radiation Research Institute (JASRI), Hyogo 679-5198 Japan*
[3]*UVSOR Synchrotron Facility, Institute for Molecular Science, Okazaki 444-8585, Japan*

This study aims to develop a mid-infrared super continuum laser (MIRS)-based infrared spectro-microtomography (IR-CT) for the purpose to understand the three-dimentional distributions of water and organic matter in extraterrestrial samples with micrometer-scale spatial resolution.

In our previous studies (FY2019-2022), we established an alignment procedure to guide the laser source to the microscope for micro-spectroscopy, adjusted the beam size at the microscope focal point, developed the sample holding technique, and conducted a two-dimentional FTIR imaging of the standard samples (e.g., calcium carbonate) by the laser. In this study, we have conducted infrared imaging by rotating the samples.

A milled bread crumb grain (~ 90 μm in longitudinal) was used as a sample. The sample was glued to the tip of a glass capillary and mounted on a gonio stage. Infrared imaging of the sample has been conducted by a JASCO IRT-7000FT-IR microscope with linear array MCT detector attached to a JASCO FT/IR-6100 at a beam line 6B, UVSOR. A MIRS laser (COVERAGE, NOVAE Laser, 1.9-3.9 μm wavelength) was used as an IR light source (Fig. 1).

The infrared images of the sample at 3022-3433 cm^{-1} have been successfully acquired every five degrees (Fig. 3). We were also able to confirm that the infrared maps reflect the sample shapes (Fig. 2). In the future study (FY2024), we will apply this approach to meteorite samples and will conduct a three-dimentional construction of the acquired data.

H.Y. and Y. I are supported by KAKENHI from the Japan Society for the Promotion of Science (JSPS) (grant no. 19H01954).

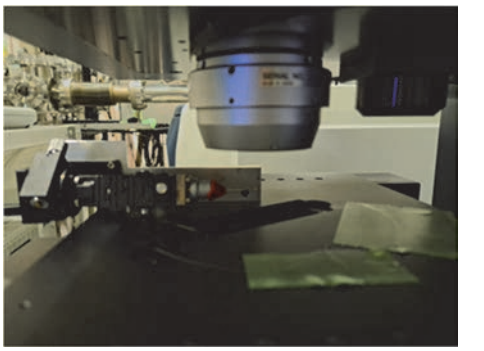

Fig. 1. Photograph of the gonio stage mounted on the microscope.

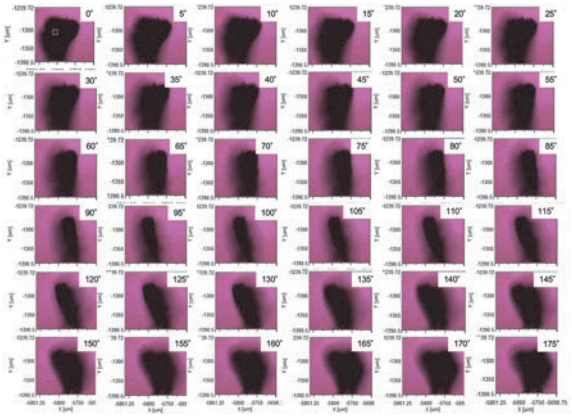

Fig. 2. Optical microscopic images of the sample (a milled bread crumb grain) taken at the rotation step in five degrees (5°).

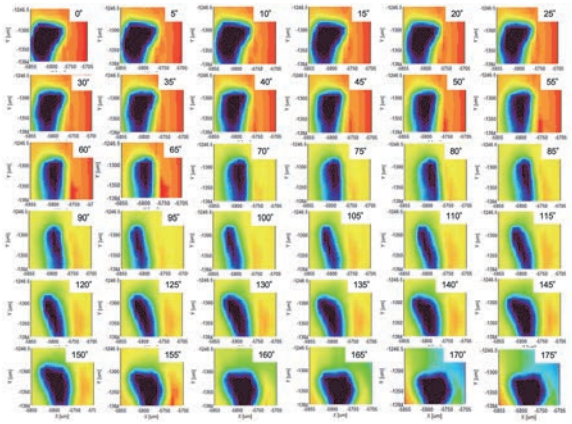

Fig. 3. Infrared images of the sample (a milled bread crumb grain) at 3022-3433 cm^{-1} taken at the rotation step in five degrees (5°).

BL6B

Structural Analysis of Amyloid Oligomers by Using Synchrotron Radiation Infrared Microspectroscopy

T. Kawasaki[1], F. Teshima[2] and K. Tanaka[2]

[1]*Accelerator Laboratory, High Energy Accelerator Research Organization, 1-1 Oho, Tsukuba, Ibaraki 305-0801, Japan*

[2]*UVSOR Synchrotron Facility, Institute for Molecular Science, 38 Nishigo-Naka, Myodaiji, Okazaki 444-8585, Japan*

We investigated protein conformations by using synchrotron radiation infrared (IR) microspectroscopy at BL6B [1]. As a model sample, we targeted hair keratin that has similar fibrillar structure with amyloid oligomers [2]. Previously, we found that keratin and amyloid fibrils can be mode-selectively dissociated by infrared free electron laser (FEL) irradiation at mid-infrared wavelengths [3]. However, the effect of near-IR FEL on the fibrillar proteins has not yet been examined.

For the measurement of IR absorption spectra in the mid-IR region, IRM-7000 infrared microscope combined with FT/IR-6100 spectroscope (Jasco Co.), which covers 350 to 15,000 cm^{-1} (45 meV-1.8 eV) was used. Samples were added on a metal-coating plate, and the measurement was performed by reflection mode with 128 scans. The resolution is about 0.5 cm^{-1}. Observation was performed by using 16 x Cassegrain lens, and the aperture size was set to 50 μm x 50 μm. The mid-IR spectra were recorded from 700 to 4000 cm^{-1}. The 2D imaging for the protein secondary conformations were performed by the lattice measurement method where x-axis is 2 points and y-axis is 2 points, and total four spectra were acquired. Protein secondary conformation analysis was performed as follows [4]: The amide I band was divided into four bands: α-helix (1650–55 cm^{-1}), β-sheet (1625–40 cm^{-1}), turn (1655–75 cm^{-1}), and non-ordered conformation (1645–50 cm^{-1}). The peak distribution corresponding to each protein conformation was visualized using the universal RGB code.

It was observed that the FEL irradiation at 3.0 μm corresponding to stretching vibrational mode of hydroxy group (νO-H) induced bending of a hair (Fig. 1). 2D protein conformational mapping analysis showed that α-helix and turn conformations are dominant compared to β-sheet and other conformations before the irradiation (left panel). On the other hand, β-sheet and other conformations were increased compared to α-helix and turns in the bending areas after the irradiation (right panel). Therefore, the near-IR FEL irradiation induced drastic conformational change of keratin, which produces the fibrillar structure containing more β-sheet conformation.

This study first shows the irradiation effect of near-IR FEL on the fibrillar conformation of proteins by using infrared imaging technique with synchrotron radiation infrared microspectroscopy analysis.

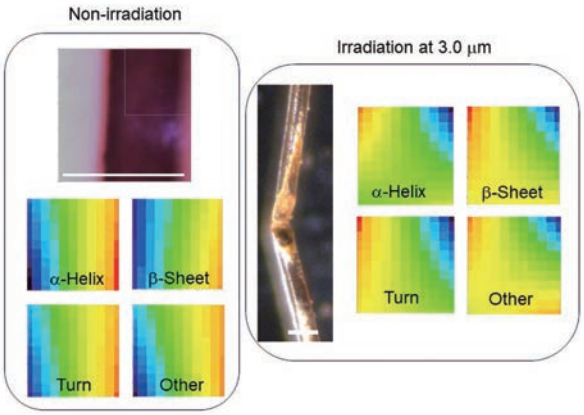

Fig. 1. 2D protein conformation imaging analysis. Left panel: non-irradiation hair sample. Right panel: hair sample after irradiation at 3.0 μm. White bar: 100 μm.

[1] S. Kimura *et al*., Infrared Phys. Technol. **49** (2006) 147.
[2] T. Kawasaki *et al.*, J. Synchrotron Radiat. **23** (2016) 152.
[3] T. Kawasaki *et al.*, J. Phys. Chem. B **124** (2020) 6266.
[4] S. Caine *et al*., Neuroimage **59** (2012) 3624.

BL7B

Study of Laboratory Simulated Space Weathering Effects on PAHs

S. Liu[1], K. Inoue[2], C. Wu[1], S. Teramoto[1] and I. Yoshikawa[1,2]
[1]*Department of Complexity Science and Engineering, Graduate School of Frontier Sciences, The University of Tokyo, Chiba 277-8561, Japan*
[2]*Department of Earth and Planetary Science, Graduate School of Science, The University of Tokyo, Tokyo 113-0033, Japan*

Polycyclic aromatic hydrocarbons (PAHs), composed solely of carbon and hydrogen, are widespread compounds in the cosmos. The PAH Hypothesis suggests a correlation between the absorption band of Interstellar Medium detected around 210 nm, attributed to PAHs, and the 217.5 nm absorption band evident in interstellar extinction curves.[1] Additionally, objects enduring exposure to outer space undergo space weathering, which alters their physical and optical properties. One notable effect of this process is the absorption bands of such objects may shift towards longer wavelengths after exposure. Utilizing ultraviolet irradiation for space weathering simulation provides a highly efficient and controllable approach.

In this study, we employed UV irradiation experiments using 0th-order light on two types of PAHs, coronene and anthracene. Subsequently, we utilized beamline BL7B to measure the transmittance spectra of the samples exposed to 0th-order light and samples exposed to the Deuterium Lamp.

In the irradiation experiments, coronene samples were subjected to irradiation for durations of 1 hour and 6 hours, while anthracene samples were exposed for 1 hour and 3 hours, employing the 0th-order light from BL7B. Notably, a thinning tendency was observed in the anthracene samples following prolonged irradiation. A Quadrupole Mass Analyzer was utilized to measure the Mass to Charge ratio within the range of 1 to 200. This enabled the analysis of potential ejecta emanating from the sample surfaces.

Following this, the transmittance spectra of the samples were measured using a photodiode. To minimize the possible impact of higher-order light, measurements were conducted across several distinct wavelength regions employing various gratings and filters.

Due to the thin total thickness of both samples and substrates, reflectance is significantly lower than transmittance. Hence, in calculations, it is permissible to approximate the absorptance ratio as 100% minus the transmittance ratio. Consequently, the data presented in Fig.2 can be derived.

The results in Fig. 2 suggest that the 12-hour exposure to deuterium lamp irradiation potentially impacts coronene's absorption spectra, indicating a shift towards shorter wavelengths and a possible decrease in absorptance. This aligns with previous space weathering research findings.[2] The observed shift could be due to hydrogen atom loss. Future research will involve analyzing mass spectrometer data from the irradiation experiment and conducting theoretical calculations for further confirmation.

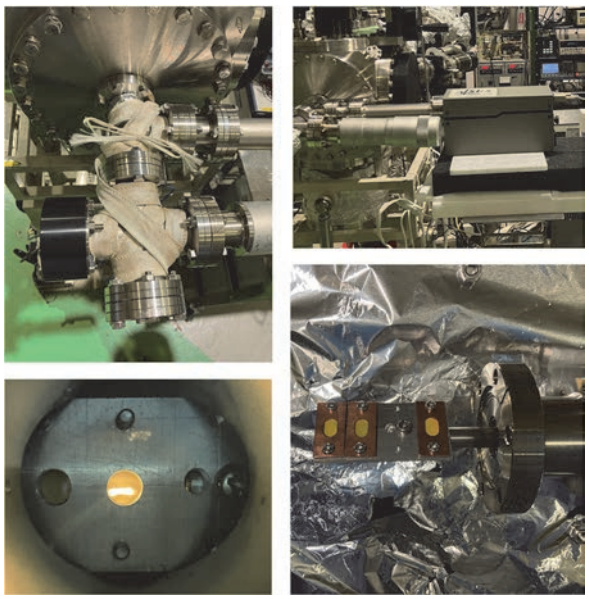

Fig. 1. Irradiation experiment.

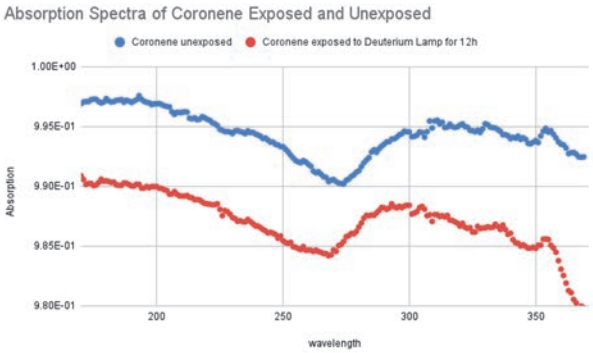

Fig. 2. Absorption spectra of coronene exposed and unexposed.

[1] C. Joblin *et al*., Astrophys. J. **393** (1992) L79.
[2] S.K. Noble, C.M. Pieters and L.P. Keller Icarus **192** (2007) 629.

UVSOR User 8